



Numerical Analysis on Pipeline Leakage Characteristics for Incompressible Flow

Y. Zeng and R. Luo

National Metrology Centre, 1 Science Park Drive, Singapore, Singapore, 118221, Singapore

†Corresponding Author Email: zeng_yan@nmc.a-star.edu.sg

(Received November 22, 2017; accepted September 28, 2018)

ABSTRACT

Systematic Computational Fluid Dynamics (CFD) simulations on incompressible water pipe flow with leakage were conducted in the present study. The aim is to provide the understanding of how different parameters, including the leakage pipe diameter, inlet mass flow rate, and main pipe length, affect the flow phenomena at the vicinity of the leakage location. The present CFD data show that the leakage pipe diameter has dominant effect on the leak mass quantity, pressure change at the vicinity of leak location, total pressure drop and pressure gradient along the main pipe. The effects of both inlet mass flow rate and the main pipe length on leak mass quantity are comparably important. Due to existence of the leakage pipe, larger velocity but lower pressure at upstream, and lower velocity but larger pressure at downstream occur at the vicinity of leakage, which causes adverse pressure at this region. The pressure change resulted from the adverse pressure increases approximately linear with the leak size ratio (ratio of leakage pipe diameter to main pipe diameter) when it is smaller than approximately 40%, at which the maximum pressure change at the leak location occurs. When the leak size ratio is smaller than approximately 5%, the pressure change at the leak location is seen to be approximately zero, implying negligible pressure difference at the two boundary points of leakage pipe. There is sudden change in the pressure gradient along the flow direction at the leak location, which results from a local pressure increase there. When farther away from the leakage, the magnitude of the maximum pressure gradient along the flow direction is reduced due to attenuation of leakage effect. The present study proves that CFD analysis could be an effective and less-costly way to investigate pipe flow with leakage, so as to provide scientific understanding of the physics on pipe flows with leakage.

Keywords: Incompressible flow; Pipeline with leakage; Numerical analysis; Leakage characteristics.

NOMENCLATURE

A^*	leak area ratio	m_{in}	inlet mass flow rate
d	diameter of the main pipe	m_L	leak mass flow rate
dL	diameter of the discharge pipe for leakage	m_L^*	leak quantity ratio
dL^*	leak size ratio	u	velocity in x direction
DP_T	pressure drop along the main pipe	v	velocity in y direction
DP_L	pressure change at the vicinity of leak location	w	velocity in z direction
L	the length of the main pipe	x	spanwise direction
$PL@up$	pressure at upstream of leak location	xL	leak location
$PL@down$	pressure at downstream of leak location	y	vertical direction
$P_{out}@main$	pressure at the outlet of the main pipe	z	flow direction
$P@Z1$	pressure at $z1=0.05m$	ρ	density of water
$P@Z2$	pressure at $z2=1.50m$	μ	dynamic viscosity of water

1. INTRODUCTION

Pipeline transportation is an efficient and economic means to convey the transport of gas, oil and water. However, due to corrosion and pressure surges, the

pipeline rupture cannot be avoided which leads to leaks in pipeline, and thus risks associated with accidental releases of transported product are still high (da Silva *et al.*, 2005; Costa, *et al.*, 2001).

Fluid leakage may cause serious pollution, injuries, and fatalities. In deepwater operation which is an important part of producing oil and gas supplies, leakage from subsea pipelines has been a serious problem, because of its potential threat to surrounding marine environments, significant monetary loss from the delay of hydrocarbon production, and difficulty in detection and remedial processes (Kam, 2010). The problem of leakage is also serious for water pipelines including fresh water supply as well as waste water treatment which may cause not only waste of water resources but also waste water contamination to the environment (Liggett and Chen, 1994; Vitkovsky *et al.*, 2001; Kim *et al.*, 2008). Delay in leak detection of water pipeline may lead to environmental health disasters.

Delay in leakage detection and repair of a failed water pipe may also cause significant water loss and serious damage to infrastructure near the failure. The amount of non-revenue water has been reported to be 15.2-35.1% of drinking water supply in United States (<http://nepis.epa.gov/>), 6.5-24.6% in Europe (<http://www.ndew.de/>), and 4.3-27.0% in Korea (<http://me.go.kr/>). These losses can be classified into unbilled public usage, apparent losses which include unauthorized consumption and metering inaccuracies, and real losses through overflows at storage tanks and burst leaks in distribution pipelines which were caused by bad connections, pipe corrosion, and physical damages (Choi *et al.*, 2017). Therefore, early detection of leakage in water pipeline is of great importance to reduce water production costs and to protect the safety of public (Puust *et al.*, 2010; Ishido and Takahashi, 2014; Martini *et al.*, 2015).

Many leak detection and localization techniques and methods have been developed and investigated, which can be generally classified into three categories, biological, hardware, and software methods (Murvay and Silea, 2012; Shehadeh and Shahata, 2013) based on the technical nature. Biological methods, referred to as non-technical methods, use trained animals such as smell-sensitive dogs and pigs to find out the leak locations along the pipeline. Hardware methods mainly rely on the usage of special sensors or devices to detect leak locations. Further classification can be made depending on the type of sensors or devices used for detection (Shehadeh and Shahata, 2013). Software methods use computer programs to monitor the evolution of pipeline parameters such as pressure, temperature, flow rate and so on, so as to infer whether leak occurs or not.

Among all the leak detection methods, the most popular approach for water leakage is to install acoustic/vibration sensors or pressure transducers (Choi *et al.*, 2017). With the utilization of two sensors, the leak can be located by estimating the time difference through correlation of the signals received. The accuracy of the time difference estimation schemes based on spectral transform can be improved by the short-time Fourier transform (STFT) and wavelet transform (Lay-Ekuakille *et al.*, 2009; Ge *et al.*, 2009), and the correlation-based

leak detector has been verified via hardware implementation (Zhang *et al.*, 2013). Based on vibration sensors and generalized cross-correlation techniques, a new method to detect and locate leakage in water pipes was proposed by Choi *et al.* (2017). With the adoption of a modified maximum-likelihood (ML) prefilter with a regularization factor, this method outperforms the conventional techniques by the verification from field measurements.

With the development of high performance computing, Computational Fluid Dynamics (CFD) simulations have been applied to investigate pipeline flows. Olivares (2009) conducted two- and three-dimensional simulations to investigate turbulence flow and acoustics induced in heating water pipes. It was found that eddies induced by leakage cause pipe acoustics. Ben-Mansour *et al.* (2012) conducted numerical simulations on small leaks in water pipelines with three different rectangular shapes of leakage: 1mm × 1mm, 2mm × 2mm, 1mm × 10mm. The results showed that the presence of a leak causes measureable differences in the magnitude and frequency of the pressure signal spectrum in the range of 220-500Hz. Barbosa *et al.* (2012), numerically studied three-phase flow (heavy oil, water and gas) in vertical pipeline using ANSYS-CFX. The results showed that the effect of small leak on the velocity and temperature distribution along the pipe can be negligible. de Sousa *et al.* (2013) studied hydrodynamic of two-phase (oil-water) flow in vertical pipe with a leakage by using ANSYS-CFX. It was concluded that volumetric fraction of phases and fluid mixture velocity affect pressure drop and mass flow rate at the leak hole. Shehadeh and Shahata (2013) carried out CFD analysis to study incompressible pipeline flow with leakage under different rupture diameters and fluid flow properties. The numerical results showed that leaks at high Reynolds number may be detected more easily than at lower Reynolds number. de Vasconcellos Araújo *et al.* (2014) conducted simulations to investigate hydrodynamic characteristics in oil pipe. The velocity field for two leaks at different locations were reported. The results revealed that the leak closer to the inlet would generate higher pressure drop. CFD analysis was carried out by Jujuly (2016) to study steady and transient pipe flow with leakage for four different fluids: methane, nitrogen, water, and crude oil. Comparisons among the four different flow media and three different leak sizes were conducted. Water flow behavior in the pipe with leakage, as well as induced acoustics, were investigated at different leak locations to give insights into flow characteristics near the leak region. A recent study by Zeng and Luo (2017) numerically investigated the water flow phenomena in a short pipe with leakage. The results showed that the relationship between the pressure change at the upstream and downstream of the leak location and leak mass flow rate is approximately linear, with dominant effect of the inlet mass flow rate and negligible effect of the pipe length. All these numerical studies have verified that CFD simulation could be an effective and efficient way to provide theoretical basis to

understand the pipeline flows with leakage.

Among plenty of published references on pipeline flows with leakage, there is short of systematic investigations to explore the underline mechanism governing the leakage which is still not yet clear. In the present study, a series of systematic numerical simulations were therefore carried out to investigate incompressible pipe flow under different conditions including the inlet mass flow rate, leakage pipe diameter, and main pipe length. Moreover, a wide range of leak size ratio (ratio of the leakage pipe diameter to main pipe diameter) was included in this study to cover extensive real-field problems in engineering applications. The flow characteristics at the vicinity of the leakage in pipe flows were captured and analyzed. The simulation results could provide reference for the actual cases, and deepen the understanding of the flow phenomena and leakage characteristics for incompressible pipeline flows.

2. MODEL CONFIGURATION AND COMPUTATIONAL METHOD

A straight pipe with water as working fluid is considered in the present study, while the leakage is performed by a discharge pipe to atmosphere. All the dimensions and boundary conditions were set the same as the experimental work (Molina-Espinosa *et al.*, 2013), which has been illustrated in our previous study (Zeng and Luo, 2017). The fluid domain of the main and discharge pipes is shown in Fig. 1, with the origin of the coordinate at the center of the main pipe inlet surface.

In this study, two pipe lengths and ten discharge pipe diameters at two inlet mass flow rates have been taken into account, while the diameter of the main pipe, leakage location, and the pressure at outlet remain unchanged. The length of the discharge pipe is longer than 5 times of its diameter to make the flow fully developed so as to make use of ambient pressure condition at its outlet. The dimensions and boundary conditions are listed in Table 1.

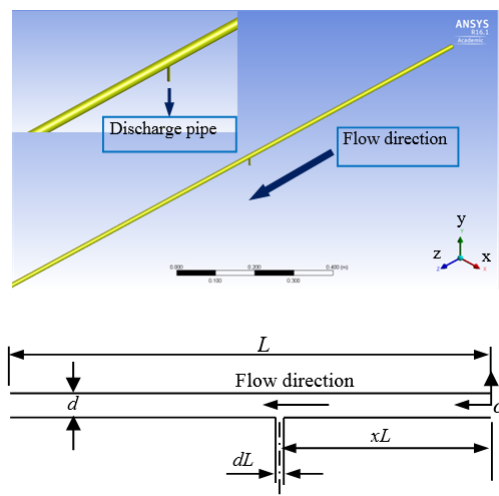


Fig. 1. 3D and 2D configurations for the main and discharge pipes.

Table 1 Pipe sizes and flow boundary conditions

Boundary conditions	xL (m)	d (mm)	$P_{out@main}$ (Pa)	m_{in} (kg/s)	L (m)	dL (mm)
Mass flow inlet & Pressure outlet	0.73	12.7	81	0.13 & 0.32	2.23 & 3.35	0
						0.635
						0.953
						1.27
						1.588
						1.91
						2.54
						3.2
						5.2
						7.2
10						
Note that $dL = 0$ represents no-leak case.						

Three-dimensional governing equations for steady state, incompressible flow in Cartesian coordinate are expressed as:

$$\frac{\partial u}{\partial x} + \frac{\partial v}{\partial y} + \frac{\partial w}{\partial z} = 0 \quad (1)$$

$$\rho \left(u \frac{\partial u}{\partial x} + v \frac{\partial u}{\partial y} + w \frac{\partial u}{\partial z} \right) = -\frac{\partial P}{\partial x} + \mu \nabla^2 u$$

$$\rho \left(u \frac{\partial v}{\partial x} + v \frac{\partial v}{\partial y} + w \frac{\partial v}{\partial z} \right) = -\frac{\partial P}{\partial y} + \mu \nabla^2 v \quad (2)$$

$$\rho \left(u \frac{\partial w}{\partial x} + v \frac{\partial w}{\partial y} + w \frac{\partial w}{\partial z} \right) = -\frac{\partial P}{\partial z} + \mu \nabla^2 w$$

CFD software ANSYS FLUENT (2013) was utilized to solve steady three dimensional (3D) Navier–Stokes equations to capture the flow phenomena. In the present study, the Reynolds number (Re) ranges over $1.2 \times 10^7 \sim 3.2 \times 10^7$ which is much larger than critical value for the turbulent pipe flow. Therefore, the flow is turbulent and the k-ε turbulence model was adopted due to its applicability for fully developed flow with fast convergence. The k-ε turbulence model, which is numerically robust and stable, can provide fairly reasonable result and has been widely used for industrial applications including pipe flow with leakage (Barbosa *et al.* 2012; de Sousa *et al.* 2013; Jujuly, 2016). SIMPLE algorithm was employed for pressure-velocity coupling. Second order discretization scheme was employed for flow variables, turbulent kinetic energy and turbulent dissipation rate.

Note that in actual conditions, small leak may often happen which could be difficult to be detected and located. Therefore, small step of variation in small leak size ratio (below 3.2mm) is considered to capture the slight change of small leak mass quantity, which could be a reference for the actual cases.

Table 2 Mesh elements and mesh quality

Mesh details	Set I	Set II	Set III
Number of elements	356,553	479,962	619,332
Minimum mesh size close to the leak tube (m)	0.0001656	0.00016580	0.0001476
Maximum mesh size (m)	0.001567	0.0013832	0.001321
Maximum aspect ratio	15.5621	14.9335	15.8503
Maximum skewness	0.7403	0.7243	0.7447
Minimum orthogonal quality	0.2023	0.2037	0.2001

Notes:
 1. Skewness from 0 to 1, where the values close to 1 correspond to low quality.
 2. Orthogonal quality from 0 to 1, where the values close to 0 correspond to low quality.

3. RESULTS AND DISCUSSION

3.1 Grid-Independent Study

To conduct mesh-independent study, three sets of tetrahedral mesh were generated by ANSYS meshing for the case of inlet mass flow rate 0.13kg/s, main pipe length 3.35m, and discharge pipe diameter 5.2mm. The mesh topology near the leakage pipe region is shown in Fig. 2. It is seen that finer mesh was generated at the leak pipe and the region close to the leak pipe, as well as coarser mesh along the main pipe with smooth transition. The mesh elements and mesh quality are listed in Table 2. The velocity magnitude variation and static pressure variation curves along the line which is 3mm above the leakage along the main pipe under different sets of mesh are presented in Fig. 3. Based on mass conservation, it is expected that velocity magnitude nearly keeps constant before and after the leak location while the value is decreased after leakage due to water flowing out through the leakage pipe, as shown in Fig. 3(a). A sudden change is found for the static pressure curves at the leak location (Fig. 3(b)). The velocity variation and static pressure variation curves obtained from different sets of mesh nearly overlap, which indicates the coarsest mesh can produce the grid-independent results. However, to make the simulation more accurate, the finest mesh (Set III with 619,332 mesh elements) was selected to conduct the simulations. For other cases with different dimensions, the same mesh resolution was applied.

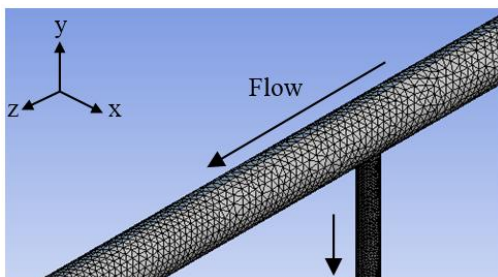


Fig. 2. Mesh Topology at the leakage pipe region.

In the present study, the convergence criteria were set as the residuals of 10^{-3} for continuity, turbulent kinetic energy as well as turbulent dissipation rate,

and 10^{-6} for velocities. A typical example for the residual change with iteration steps is shown in Fig. 4. For all the simulations cases, after around 2000 – 4000 iterations, all the residuals already reduce to the set values, and the converged results are obtained.

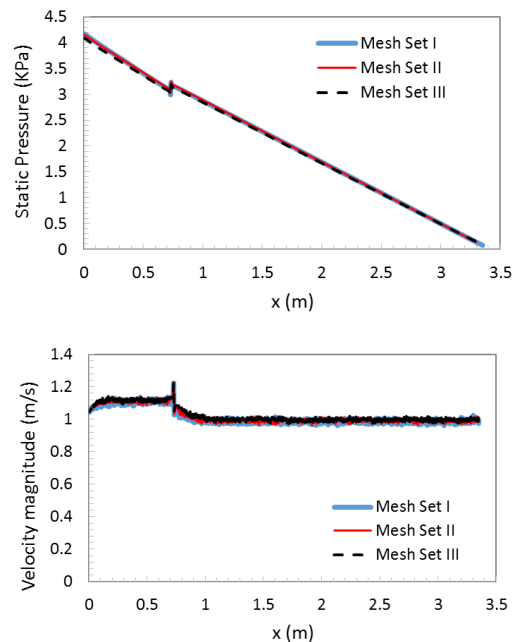


Fig. 3. (a) Velocity variation and (b) static pressure variation curves along the line which is 3mm above the leakage along the pipe under three sets of mesh for the case of inlet mass flow rate 0.13kg/s, main pipe length 3.35m, and discharge pipe diameter 5.2mm.

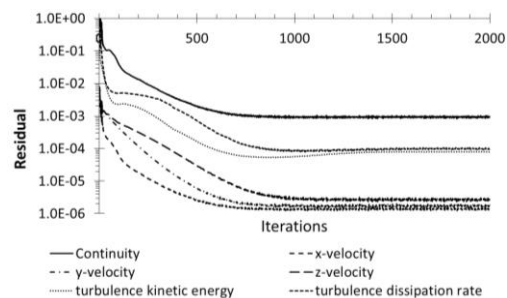


Fig. 4. The trend of residual .vs. iteration for the case of inlet mass flow rate 0.13kg/s, main pipe length 3.35m, and discharge pipe diameter 5.2mm.

Table 3 Comparison of present CFD and the reference experimental data (Molina-Espinosa *et al.*, 2013)

Conditions	DP (KPa) = P@Z1 - P@Z2		$m_L^* = m_L/m_{in}$	
	CFD	EXP	CFD	EXP
$L=3.35m$ $dL=3.2e-3m$ $m_{in}=0.13kg/s$	CFD	1.76	CFD	10.51%
	EXP	1.35	EXP	8%
	Dif (%)	30.37%	Dif (%)	31.38%
$L=2.23m$ $dL=5.2e-3m$ $m_{in}=0.32kg/s$	CFD	6.5	CFD	16.34%
	EXP	6	EXP	17%
	Dif (%)	8.33%	Dif (%)	3.88%
$L=2.23m$ $dL=7.2e-3m$ $m_{in}=0.32kg/s$	CFD	5.31	CFD	26.34%
	EXP	4.6	EXP	31%
	Dif (%)	15.43%	Dif (%) <td 15.03%	
$L=2.23m$ $dL=1.0e-2m$ $m_{in}=0.32kg/s$	CFD	4.18	CFD	38.03%
	EXP	3.5	EXP	49%
	Dif (%)	19.43%	Dif (%)	22.39%

Note that Dif (%) = |(CFD-EXP)/EXP * 100%

3.2 Model Validation

Several cases in the experimental work (Molina-Espinosa *et al.*, 2013) were selected to validate the present CFD modelling. The pressure drop at the two locations ($z1=0.05m$ and $z2=1.5m$ from the inlet) and the leak mass quantity between the present simulation and the reference experimental data (Molina-Espinosa *et al.*, 2013) are compared and listed in Table 3, which has been shown in the previous study (Zeng and Luo, 2017). The deviation between CFD and experimental data is within the range of 3.88% - 31.38%, with the smallest difference for middle leakage mass quantity ratio of 17% and the largest difference for small leak mass quantity of 8%, which is reasonable because it is more difficult to capture small leak mass quantity by both experiments and simulations due to uncertainty in experiments and computation error in simulations.

3.3 Flow Patterns

Figure 5 shows the flow and pressure contours in the vicinity of the leakage at the center plane along the flow direction under the condition of inlet mass flow rate of 0.32 kg/s, main pipe length of 3.35m and discharge pipe diameter of 5.2mm. Lower pressure at the upstream but higher pressure at the downstream of the leak can be observed, which is due to lower flow velocity downstream resulted from leak. The trend is consistent with the reference simulation results (Ben-Mansour *et al.*, 2012) and experimental data (Molina-Espinosa *et al.*, 2013).

To further understand the flow characteristics in the vicinity of the leakage, 3D Streamline and velocity vector plots at this region are shown in Fig. 6 and Fig. 7 respectively, for the same case with inlet mass flow rate of 0.32 kg/s, main pipe length of 3.35m, and discharge pipe diameter of 5.2mm.

Consistent with Fig. 5(a), the results of 3D streamline (Fig. 6) and velocity vector plot (Fig. 7(a)) at the vicinity of leakage clearly show that part of water smoothly flows through the new outlet with smaller diameter (leakage pipe), leading to

larger velocity and lower pressure at the upstream of the leakage location. At the downstream of the leakage location, there is a lower velocity region which causes higher pressure there. Thus, adverse pressure occurs at the vicinity of leakage which results in a sharp change in the pressure variation curve along the flow direction.

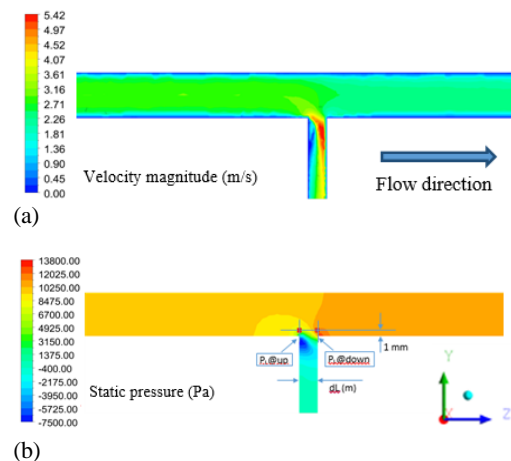


Fig. 5. (a) Velocity magnitude contour and (b) pressure contour at Centre Plane ($X=0$) in the vicinity of leak-location under the conditions of inlet mass flow rate 0.32kg/s, main pipe length 3.35m, and discharge pipe diameter 5.2mm.

The flow velocity close to the leakage pipe varies the most as shown in Fig. 7(b), showing the most significant leakage effect there. With the plane moving upward and farther away from the leakage, the velocity variation is reduced, which confirms that the leakage effect is diminishing.

To show the pressure change at the vicinity of the leak location more clearly, Fig. 8 depicts the static pressure contours at three different XZ planes: Plane XZ1 with $y = -5.35mm$ (1mm above the leakage pipe), Plane XZ2 with $y = -3.35mm$ (3mm above the leakage pipe), and Plane XZ3 with $y = 0$ (centerline plane and 6.35mm above the leakage

pipe) for the same case under those conditions indicated in Figs 5-7. Similar to the leakage effect on the flow velocity (see Figs. 7(b) – 7(d)), the pressure change near the leakage pipe is more significant and gradually reduces when the plane is moving upwards to the centerline of the main pipe, indicating that the effect of the leakage decreases. If the plane continuously moves upward, the effect of the leakage will reduce to be negligible eventually (data not shown).

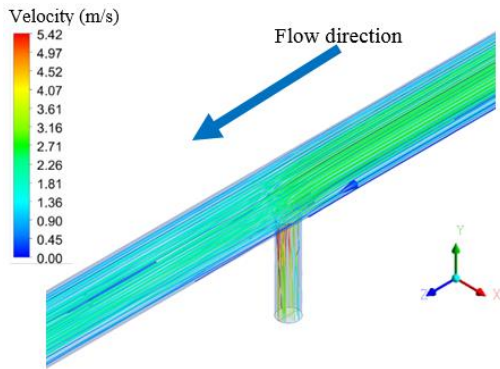


Fig. 6. 3D streamline at the vicinity of leakage pipe.

The variation curves of the static pressure along the centerline of the above three XZ planes are presented in Fig. 9. A sudden change in the static pressure can be observed, which is caused by the adverse pressure occurring at the upstream and downstream of leak location. The pressure change decreases with an increase in the distance between the plane and the leakage pipe, confirming that the leakage effect is reducing. The results are consistent with the results shown in Figs. 5-8. Compared with the reference simulation data (Ben-Mansour *et al.*, 2012), the pressure change along the centerline of the Plane XZ3 ($y = 0$ mm) still exists in the present study, which could be due to smaller diameter of the main pipe and thus larger domain that can be affected by the leakage effect.

3.4 Leakage Quantity Ratio

Leakage mass quantity ratio (m_L^*) at different conditions are summarized in Table 4.

As expected, leakage mass quantity ratio increases with increasing the leak size (or area) ratio when the other conditions remain unchanged, indicating the key effect of the leak size (or area) ratio. The effects of both the inlet mass flow rate and main pipe length are comparable. For the same inlet mass flow rate, at the leak size ratio larger than 7.5% (corresponding to the area ratio 0.56%), larger leak mass quantity ratio are observed at longer main pipe due to larger driven force, which will be explained later. For the same main pipe length, higher inlet mass flow rate causes larger driven force and larger leakage mass quantity, but the leak quantity ratio may be reduced based on larger denominator. It is worth mentioning that for the leak size ratio below 5% (corresponding area ratio 0.25%), the leak mass quantity may not be predicted accurately by present simulations, which could be due to the poor mesh quality under this condition. If the

mesh quality can be enhanced, the leak mass quantity can be predicted at even a smaller leak size ratio.

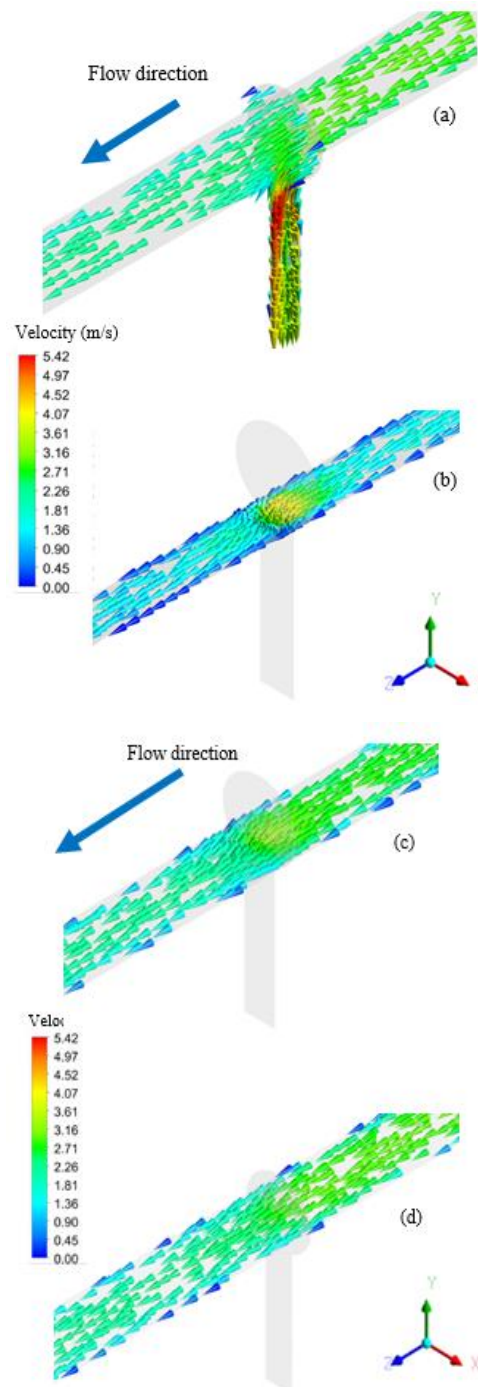


Fig. 7. Velocity vector plots at different planes (a) Plane YZ ($x = 0$) and Plane XY ($z = 0.73$ mm), (b) Plane XZ1 ($y = -5.35$ mm), (c) Plane XZ2 ($y = -335$ mm), and (d) Plane XZ3 ($y = 0$), in the vicinity of leakage under the conditions of inlet mass flow rate 0.32kg/s, main pipe length 3.35m, and discharge pipe diameter 5.2mm.

3.5 Pressure change

Figures 10 shows the effect of leak size ratio on total pressure drop along the main pipe (DP_T) at different It is

Table 4 Leakage quantity ratio at different conditions

dL^* (%)	A^* (%)	m_L^*		m_L^*	
		$m_{in} = 0.13$ (kg/s)		$m_{in} = 0.32$ (kg/s)	
		$L=3.35m$	$L=2.23m$	$L=3.35m$	$L=2.23m$
0	0.00%	0	0	0	0
5.00%	0.25%	0.071%	0.077%	0.090%	0.125%
7.50%	0.56%	0.422%	0.270%	0.417%	0.333%
10.00%	1.00%	0.980%	0.688%	0.990%	0.863%
12.50%	1.56%	1.858%	1.317%	1.767%	1.540%
15.00%	2.26%	2.900%	2.265%	2.757%	2.070%
20.00%	4.00%	5.162%	3.911%	5.571%	4.008%
25.20%	6.35%	10.510%	8.000%	9.640%	7.000%
40.94%	16.76%	23.100%	18.520%	21.130%	16.340%
56.69%	32.14%	36.320%	30.060%	33.750%	26.340%
78.74%	62.00%	53.380%	44.150%	47.880%	38.030%

observed that for the lower inlet mass flow rate of 0.13kg/s, the main pipe length approximately has negligible effect on DP_L with the two curves nearly overlapping. For the larger inlet mass flow rate of 0.32 kg/s, the main pipe length effect is more significant, especially for the leak size ratio larger than 15% (corresponding to the area ratio 2.25% and the leak mass quantity ratio 2 ~ 2.8%). The pressure change at the vicinity of leak location can be neglected for leak size ratio smaller than 5%, corresponding to area ratio of 0.25%, and leak quantity ratio of approximately 0.07 ~ 0.13%.

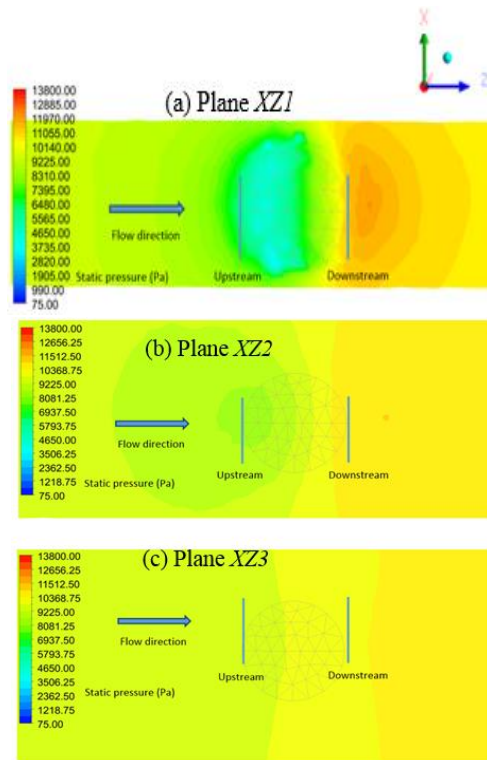


Fig. 8. Static pressure contours at different planes (XZ1, XZ2, XZ3) in the vicinity of leak-location under the conditions of inlet mass flow rate 0.32kg/s, main pipe length 3.35m, and discharge pipe diameter 5.2mm.

3.6 Pressure Gradient

The pressure gradient along the three centerlines of

the above three XZ planes is shown in Fig. 12. Compared with the static pressure variation depicted in Fig. 7, the magnitude of pressure gradient at the leak location is much larger, which indicates the most rapid change in the rate of the pressure there. The sudden change in the pressure gradient at the leak location is because the local pressure increases there, representing the typical characteristic in leak flows. It inlet mass flow rates and pipe lengths. Consistent trends show that with an increase in the leak size ratio with other conditions unchanged, total pressure drop is reduced which could be due to more mass of water flows through larger discharge pipe at larger leak size, leading to lower velocity, higher pressure at the outlet of the main pipe, and thus lower total pressure drop. Moreover, with higher inlet mass flow rate but other conditions remain the same, larger driven force is needed to push larger quantity of water, the inlet pressure is increased which causes larger pressure drop along the main pipe. Similarly, with longer main pipe but other conditions remain the same, larger driven force is needed to overcome larger resistance along the main pipe, the inlet pressure and pressure drop along the main pipe are both increased.

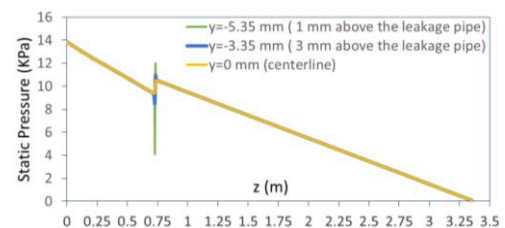


Fig. 9. Static pressure variation curves along centerlines at different planes (XZ1, XZ2, and XZ3) under the conditions of inlet mass flow rate 0.32kg/s, pipe length 3.35m, and discharge pipe diameter 5.2mm.

The pressure change between upstream and downstream of leakage location (DP_L), at different inlet mass flow rate and pipe length are summarized relative to the leak size ratio and leak quantity ratio, as shown in Fig. 11. The upstream and downstream of leakage locations are set at the two points located 1mm above the leakage pipe and half-diameter of the leakage pipe away from the leakage pipe center, as marked in Fig. 2(b).

Table 5 Peak pressure gradient at different conditions

Planes	$m_{in} = 0.13$ (kg/s)			$m_{in} = 0.32$ (kg/s)		
	dL^* (%)	A^* (%)	m_L^*	dL^* (%)	A^* (%)	m_L^*
XZ1 (y= -5.35mm) 1mm above the leakage pipe.	40%	16%	7-10%	25%	6.25%	18-23%
XZ2 (y=-3.35mm) 3mm above the leakage pipe.	50%	25%	25%	30%	9%	12%
XZ3 (y=0mm) 5.35mm above the leakage pipe	No observation of peak pressure gradient					

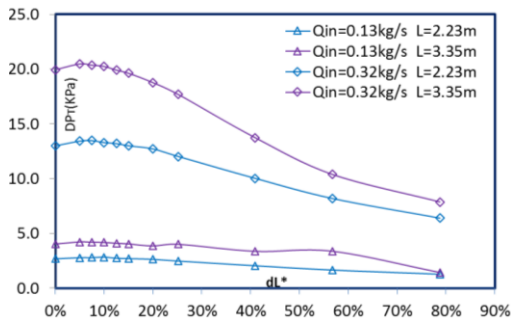


Fig. 10. Total pressure drop along the main pipe .vs. leak size ratio at different inlet mass flow rates and main pipe lengths.

Lower pressure at upstream and higher pressure at downstream of the leak lead to positive magnitude of the pressure change at the vicinity of leak location, consistent with the experimental results (Molina-Espinosa *et al.*, 2013). The increase in pressure after leak is promoted by decreasing the downstream flow rate and kinetic energy due to leak. It is seen that the pressure change at the vicinity of leak location increases nearly linearly with the leak size ratio when it is below 40%, while above that it remains nearly unchanged for the lower inlet mass flow rate and decreases for the larger inlet mass flow rate, indicating the peak pressure change at the vicinity of leak location, corresponding to the area ratio 16% and leak mass quantity ratio of approximately 20%, consistent with the data shown in Table 4.

is clearly seen that the effect of leakage decreases when the plane is farther away from the leakage pipe, consistent with the previous results shown in Figs. 7-9. The magnitude of the maximum pressure gradient decreases from 2344 *KPa/s* at Plane XZ1 (y = -5.35 mm), to 632.8 *KPa/s* at Plane XZ2 (y = -3.35 mm), and finally 166.7 *KPa/s* at Plane XZ3 (y = 0 mm). Compared with the reference simulation data (Ben-Mansour *et al.*, 2012), much larger magnitude is found in the present study, which could be probably due to smaller diameter of the main pipe and thus more significant leakage effect.

To further figure out the leakage effect, the magnitudes of the maximum pressure gradient along the three centerlines of the above three XZ planes at different leak size (or area) ratios and leakage mass quantity ratios are summarized in Table 5.

Table 5 shows the leak size (or area) ratio for the maximum pressure gradient at above three XZ planes. It is seen that with the plane moving farther away above the leakage pipe (from XZ1 to XZ2), the maximum pressure gradient will be reached at larger

leak size (or area) ratio, corresponding to higher leak mass quantity ratio. There no observation of the peak pressure gradient at Plane XZ3 (centerline plane), confirming that the leakage effect becomes more trivial with the plane being farther away from the leakage pipe. It can be summarized that the pressure gradient along the main pipe is much more obvious to be observed due to its larger magnitude, and thus it would be much more favorable to detect and locate the leakage if the pressure gradient can be measured in experiments.

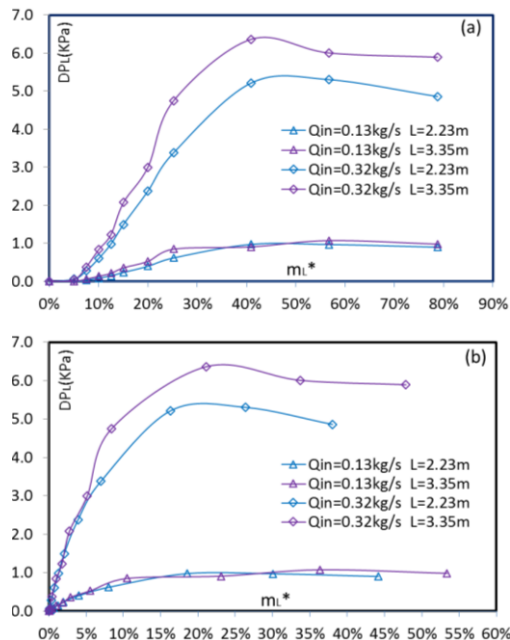


Fig. 11. Pressure change at the vicinity of leak location at different inlet mass flow rates and main pipe lengths .vs. (a) leak size ratio, and (b) leakage quantity ratio.

4. CONCLUSIONS

Systematic numerical simulations on incompressible water pipe flow with leakage were performed in the present study. Different parameters including the inlet mass flow rate, leakage pipe diameter, and pipe length were considered. The effects of these parameters on the leak mass quantity, total pressure drop along the main pipe, pressure change at the vicinity of leak location, and pressure gradient along the main pipe were investigated and analyzed. The leakage pipe diameter (represented as leak size ratio or area ratio) shows dominant effect, which is reasonable and

expected. Compared with the main pipe length, the simulation results show that the inlet mass flow rate has more significant impact. Larger velocity but lower pressure at upstream, and lower velocity but larger pressure at downstream take place at the vicinity of leakage, which causes adverse pressure with a sharp variation in pressure at this region. The pressure change at the vicinity of leak location increases approximately linearly with the leak size ratio when the ratio is smaller than approximately 40%, corresponding to the leak area ratio 16% and leak mass quantity ratio 16-23%. The pressure change at the vicinity of leak location is observed to be negligible, when the leak mass quantity ratio smaller than approximately 0.07 ~ 0.13%, corresponding to the leak size ratio 5% and area ratio 0.25%. Note that the pressure change at the vicinity of leak location actually occurs over a definite distance but not at the point of leakage location.

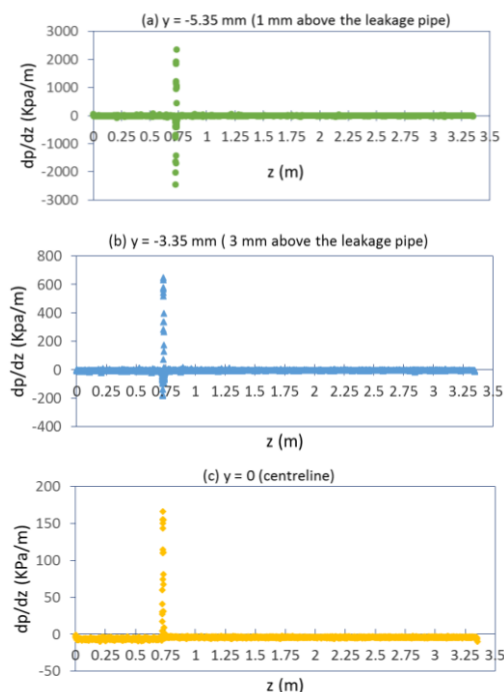


Fig. 12. Pressure gradient variation curves along centerlines at different XZ planes under conditions of the inlet mass flow rate 0.32kg/s, main pipe length 3.35m, and discharge pipe diameter 5.2mm.

Due to an increase in the local pressure at the leak location, there is a sudden change in the pressure gradient along the flow direction and the magnitude is much larger than that of the pressure change there, representing the typical characteristic of the most rapid change in the rate of the pressure change there in leak flows. From the summary of the maximum pressure gradient along flow direction, it is observed that the effect of the inlet mass flow rate is dominant compared with that of the main pipe length. It is expected that the magnitude of the maximum pressure gradient reduces with farther away from the leakage pipe, due to diminishment of the leakage effect. The present study verifies that simulation is an effective and economic tool to investigate pipe flow leakage, so as to help understand the physics of such flow

phenomena.

REFERENCES

- ANSYS Fluent 15.0 Theory Guide (2013).
- Barbosa, L.M.C., A.G.B. de Lima and S.R. Farias Neto (2012). Non-isothermal Transient Three-phase Flow (Heavy Oil, Water and Gas) in Vertical Pipeline: the Effect of Leakage. *International Journal of Modeling and Simulation for the Petroleum Industry* 6 (2), 23-31.
- Ben-Mansour, R., M. Habib, A. Khalifa, K. Youchef-Toumi and D. Chatzigeorgiou (2012). Computational fluid dynamic simulation of small leaks in water pipelines for direct leak pressure transduction. *Computers & Fluids* 57, 110-123.
- Choi, J., J. Shin, C. Song, S. Han and D. Park (2017). Leak detection and location of water pipes using vibration sensors and modified ML prefilter. *Sensor* 17, 2104.
- Costa D., I. Stoianov, D. Bulter, C. Marksimovic, N. Graham and H. Ramos (2001, September). Leak detection in a pipeline systems by inverse transient analysis: from theory to practice. In *Proceedings of International Conference on Computing and Control for the Water Industry*, Leicester. U.K.
- da Silva, H.V., C. Morooka., I. Guiherme, T. da Fonseca and J. Mendes (2005). Leak detection in petroleum pipelines using a fuzzy system. *Journal of Petroleum Science and Engineering* 49, 223-238.
- de Sousa1, J.V.N., C.H. Sodr , A.G.B. de Lima and S.R. de Farias Neto (2013). Numerical Analysis of Heavy Oil-Water Flow and Leak Detection in Vertical Pipeline. *Advances in Chemical Engineering and Science* 3, 9-15.
- de Vasconcellos Ara jo, M., S.R. de Farias Neto, A.G.B. de Lima and F.D.T. de Luna (2014). Hydrodynamic Study of Oil Leakage in Pipeline via CFD. *Advances in Mechanical Engineering* 6, 170-178.
- Ge, C., H. Yang, H. Ye and G. Wang (2009). A fast leak locating method based on wavelet transform. *Tsinghua Science and Technology* 14, 551-555.
- Ishido, Y. and S. Takahashi (2014). A new indicator for real-time leak detection in water distribution networks: design and simulation validation. *Procedia Engineering* 89, 411-417.
- Jujuly, M.M. (2016). Computational Fluid Dynamics (CFD) based approach to consequence assessment of accidental release of hydrocarbon during storage and transportation. *Master Thesis*. Memorial University of Newfoundland, Newfoundland and Labrador, Canada.
- Kam, S. (2010). Mechanistic modeling of pipeline

- leak detection at fixed inlet rate. *Journal of Petroleum Science and Engineering* 70, 145-156.
- Kim, Y., K. Miyazaki and H. Tsukamoto (2008). Leak detection in pipe using transient flow and genetic algorithm. *Journal of Mechanical Science and Technology* 22, 1930-1936.
- Lay-Ekuakille, A., G. Vendramin, A. Trotta and P. Vanderbemden (2009). STFT-based spectral analysis of urban waterworks leakage detection. In *Proceedings of the XIX IMEKO World Congress Fundamental and Applied Metrology*, Lisbon, Portugal, 6-11 September.
- Liggett, J. and L. Chen (1994). Inverse transient analysis in pipe networks. *Journal of Hydraulic Engineering* 120 (8), 934-955.
- Molina-Espinosa, L., O. Cazarez-Candia and C. Verde-Rodarte (2013). Modeling of incompressible flow in short pipes with leaks. *Journal of Petroleum Science and Engineering* 109, 38-44.
- Olivares, P.A.V. (2009). Acoustic Wave Propagation and Modeling Turbulent Water Flows with Acoustics for District Heating Pipes. *PhD Thesis*, Uppsala University, Uppsala, Sweden.
- Puust, R., Z. Kapelan, D.A. Savic and T. Koppel (2010). A review of methods for leakage management in pipe networks. *Urban Water Journal* 7, 25-45.
- Shehadeh, M. and A. Shahata (2013). Modelling the effect of incompressible leakage patterns on rupture area in pipeline. *CFD Letters* 5 (4), 132-142.
- Vitkovsky, J., A. Simpson and M. Lambert (2001). Leak detection and calibration using transient genetic algorithms. *Journal of Water Resources Planning and Management-ASCE* 126 (4), 262-265
- Zeng, Y. and R. Luo (2017, May). Numerical Analysis of Incompressible Flow Leakage in Short Pipes. In *Proceedings of International Pipeline Technology Conference*. Berlin, Germany
- Zhang, L., Y. Wu, L. Guo and P. Cai (2013). Design and implementation of leak acoustic signal correlator for water pipelines. *Information Technology Journal* 12, 2195-2200.